PM₁₀-bound trace elements in pan-European urban atmosphere

Liu, Xiansheng; Zhang, Xun; Wang, Tao; Jin, Bowen; Wu, Lijie; Lara, Rosa; Monge, Marta; Reche, Cristina; Jaffrezo, Jean-Luc; Uzu, Gaelle; Dominutti, Pamela; Darfeuil, Sophie; Favez, Olivier; Conil, Sébastien; Marchand, Nicolas; Castillo, Sonia; de la Rosa, Jesús D.; Stuart, Grange; Eleftheriadis, Konstantinos; Diapouli, Evangelia

Link to publication on Research at Birmingham portal

PM$_{10}$-bound trace elements in pan-European urban atmosphere

Xiansheng Liu [a], Xun Zhang [b,c,*], Tao Wang [d,**], Bowen Jin [b], Lijie Wu [b], Rosa Lara [a], Marta Monge [a], Cristina Reche [a], Jean-Luc Jaffrezo [e], Gaelle Uzu [e], Pamela Dominutti [e], Sophie Darfeuil [e], Olivier Favez [f,g], Sébastien Conil [h], Nicolas Marchand [i], Sonia Castillo [j,k], Jesús D. de la Rosa [l], Grange Stuart [m], Konstantinos Eleftheriadis [n], Evangelia Diapouli [n], Maria I. Gini [n], Silvia Nava [o], Célia Alves [p], Xianxia Wang [q], Yiming Xu [r], David C. Green [s], David C.S. Beddows [t], Roy M. Harrison [t], Andrés Alastuey [a], Xavier Querol [a]

[a] Institute of Environmental Assessment and Water Research (IDAEA-CSIC), 08034, Barcelona, Spain
[b] Beijing Key Laboratory of Big Data Technology for Food Safety, School of Computer and Artificial Intelligence, Beijing Technology and Business University, Beijing, 100048, China
[c] State Key Laboratory of Resources and Environmental Information System, Beijing, China
[d] Shanghai Key Laboratory of Atmospheric Particle Pollution and Prevention, Department of Environmental Science & Engineering, Fudan University, Shanghai, 200433, China
[e] Univ. Grenoble Alpes, IRD, CNRS, INRAE, Grenoble INP, IGE, UMR 5001, 38000, Grenoble, France
[f] INERIS, Parc Technologique Alata, BP 2, 60550, Verneuil-en-Halatte, France
[g] Laboratoire central de surveillance de la qualité de l'air (LCSQA), 60550, Verneuil-en-Halatte, France
[h] ANDRA DISTEC/EES Observatoire Pérenne de l'Environnement, F–55290, Bure, France
[i] Aix Marseille Univ, CNRS, LCE, Marseille, France
[j] Department of Applied Physics, University of Granada, 18011, Granada, Spain
[k] Andalusian Institute of Earth System Research, IISTA-CEAMA, University of Granada, 18006, Granada, Spain
[l] Associate Unit CSIC-UHU Atmospheric Pollution, University of Huelva, 21071, Huelva, Spain
[m] Swiss Federal Laboratories for Materials Science and Technology, Dübendorf, CH, Switzerland
[n] ENRACT, Institute of Nuclear and Radiological Science & Technology, Energy & Safety, NCSR Demokritos, 15310, Ag. Paraskevi, Athens, Greece
[o] INFN Division of Florence and Department of Physics and Astronomy, University of Florence, via G.Sansone 1, 50019, Sesto Fiorentino, Italy
[p] Department of Environment and Planning, Centre for Environmental and Marine Studies (CESAM), University of Aveiro, 3810-193, Aveiro, Portugal
[q] School of Management, Minzu University of China, Beijing, 100081, China
[r] School of Grassland Science, Beijing Forestry University, Beijing, 100083, China
[s] MRC Centre for Environment and Health, Environmental Research Group, Imperial College London, United Kingdom
[t] School of Geography Earth and Environmental Sciences, University of Birmingham, B15 2TT, Birmingham, United Kingdom

ARTICLE INFO

ABSTRACT

Although many studies have discussed the impact of Europe's air quality, very limited research focused on the detailed phenomenology of ambient trace elements (TEs) in PM$_{10}$ in urban atmosphere. This study compiled long-term (2013–2022) measurements of speciation of ambient urban PM$_{10}$ from 55 sites of 7 countries (Switzerland, Spain, France, Greece, Italy, Portugal, UK), aiming to elucidate the phenomenology of 20 TEs in PM$_{10}$ in urban Europe. The monitoring sites comprised urban background (UB, n = 26), traffic (TR, n = 10), industrial (IN, n = 5), suburban background (SUB, n = 7), and rural background (RB, n = 7) types. The sampling campaigns were conducted using standardized protocols to ensure data comparability. In each country, PM$_{10}$ samples were collected over a fixed period using high-volume air samplers. The analysis encompassed the spatiotemporal distribution of TEs, and relationships between TEs at each site. Results indicated an annual average for the sum of 20 TEs of 90 ± 65 ng/m^3, with TR and IN sites exhibiting the highest concentrations (130 ± 66 and 131 ± 80 ng/m^3, respectively). Seasonal variability in TEs concentrations, influenced by emission sources and meteorology, revealed significant differences ($p < 0.05$) across all monitoring sites. Estimation of TE

concentrations highlighted distinct ratios between non-carcinogenic and carcinogenic metals, with Zn (40 ± 49 ng/m^3), Ti (21 ± 29 ng/m^3), and Cu (23 ± 35 ng/m^3) dominating non-carcinogenic TEs, while Cr (5 ± 7 ng/m^3), and Ni (2 ± 6 ng/m^3) were prominent among carcinogenic ones. Correlations between TEs across diverse locations and seasons varied, in agreement with differences in emission sources and meteorological conditions. This study provides valuable insights into TEs in pan-European urban atmosphere, contributing to a comprehensive dataset for future environmental protection policies.

1. Introduction

Air pollution remains a silent killer in Europe. Despite significant reductions in emissions over the last two decades, it continues to pose the greatest environmental health risk, according to the European Environment Agency (EEA, 2023a). This is, in part, because atmospheric particulate matter (PM) contains a complex mixture of pollutants, with trace elements (TEs) being recognized as one of the crucial categories of PM components with the greatest health risks (Idani et al., 2020). Generally, TEs originate from various natural and anthropogenic sources, including traffic, industrial activities, and incineration (Pacyna, 1986; Rahman et al., 2019; Kumar et al., 2024). For instance, steel production emits high levels of Fe, Zn, Mn, Pb, and Cd, while tire wear and brake pad wear release Zn, Fe, Cu, Sb, and Sn into the atmosphere (Schauer et al., 2006; Querol et al., 2007; Thorpe and Harrison, 2008; Amato et al., 2009; Peikertova and Filip, 2016; Chalvatzaki et al., 2019; Charron et al., 2019).

TEs pose resistance to degradation, many of them exhibit high toxicity, and readily undergo enrichment in many environments (Faraji Ghasemi et al., 2020; Budi et al., 2024; Lafta et al., 2024). Ambient PM contains a wide range of TEs, including Mg, Al, Mn, Zn, Cu, As, Hg, Cr, Cd, Pb, Fe, among many others. Cd, As, Cr, and Ni, in particular, have been associated with carcinogenic risks (Tepanosyan et al., 2017; Sharma et al., 2022). Other TEs, such as Fe, V, Cr, Co, Ni, Cu, Zn, and Ti, can trigger oxidative stress by Fenton-type reactions (Baulig et al., 2009). Studies suggested that long-term exposure to elevated levels of air pollutants containing toxic metals is frequently associated with the development of respiratory and cardiovascular illnesses, thereby increasing the rates of both premature mortality and morbidity (Li et al., 2015; Yang et al., 2016; Moradi et al., 2022; Mohammadi et al., 2024; Seihei et al., 2024). Such repercussions encompass neurological symptoms, heightened blood pressure, anemia, kidney impairment, and an escalated susceptibility to lung and kidney cancer (Momtazan et al., 2018; Briffa et al., 2020; Tahery et al., 2021; Borsi et al., 2022; Collin et al., 2022; Abbasi-Kangevari et al., 2023). Therefore, the study of TEs abundance in atmospheric PM and their impact on human health risks has received increasing attention.

Within the European Union (EU), key policy instruments addressing air pollution include the ambient air quality Directive 2008/50/EC. This directive establishes limit values for environmental air concentrations of various pollutants, including lead (Pb) (EU, 2008). Additionally, the Directive 2004/107/EC proposes target (not limit) values for arsenic (As), cadmium (Cd), mercury (Hg), nickel (Ni), in ambient air (EU, 2004). However, for other TEs, with reported potential health effects (such as Cu, Mn, Cr, and Zn (Chen et al., 2022)), particularly trace heavy metals, the EU has not set specific targets or limits and this does not favor the measurements of these pollutants in urban areas. While the levels of TEs have been documented to be lower in major cities across Europe and the United States compared to economically advanced urban areas in developing nations (e.g., China, India), the specific concentrations of individual TEs (e.g., like Cd, as suggested by Coudon et al. (2018)) can remain elevated throughout the year. For instance, time-series analyses of Ni concentrations demonstrated no statistically significant decrease from a rural background station in Montseny (MSY) in northeastern Spain from 2009 to 2018 (In'T Veld et al., 2021). Therefore, despite the large efforts dedicated to research on atmospheric PM pollution in Europe, further studies on non-regulated TEs are

needed, especially for urban areas, where people are particularly exposed to high levels of TEs due to the contamination of air through PM$_{10}$ and PM$_{2.5}$ particles (Heidari-Farsani et al., 2013; Aksu, 2015; Sielski et al., 2021).

RI-URBANS (Research Infrastructures Services Reinforcing Air Quality Monitoring Capacities in European Urban & Industrial Areas, funded within the European Union's Horizon, 2020 research and innovation program, 101036245) is a European research project, devoted to demonstrating the applications of advanced air quality service tools in urban Europe to improve the assessment of air quality policies, including a better evaluation of health effects. In this context, this study aims to gather and evaluate the largest dataset available for PM$_{10}$-bound TEs from countries within Europe, encompassing urban background, traffic, industrial, suburban background, and rural background regions. This paper presents this achievement, with data from 55 sites across 7 countries, and includes a synthesis of concentration profiles of 20 TEs, comparing TEs concentrations among these countries and contrasting them with global TEs concentrations elsewhere. It also addresses the spatiotemporal trends of TEs within the research area across various types of locations. This work offers valuable insights into the intricated panorama/big picture of TE pollution within the European atmosphere.

2. Materials and methods

2.1. Measurement sites and dataset

This study is based on TEs data from 55 sites provided by air quality monitoring networks, research projects, and research supersites. The dataset spans a decade, covering the years 2013–2022, with series of data for each site covering a minimum of one year. The data come essentially from 7 countries: France (24 sites), Italy (9), Spain (8), Switzerland (5), UK (5), Portugal (3), Greece (1). The overall data base represents 16864 daily samples. These include (Fig. 1, Table S1):

- Twenty-six urban background (UB) sites covering most of western Europe: Basel (BAS_UB), Barcelona (BCN_UB), Florence Capannori (CA_UB), Florence Calenzano (CAL_UB), Coimbra (COIM_UB), Granada (GRA_UB), Grenoble CB (GRE-cb_UB), Grenoble FR (GRE-fr_UB), Grenoble VIF (GRE-vif_UB), Lens (LEN_UB), Lyon (LYN_UB), Madrid E. Vallecas (MAD-EV_UB), Magadino (MAG_UB), Manlleu (MAN_UB), Milano (MIL-air_UB), Milan Pascal (MIL-pas_UB), Marseille Longchamp (MRS-LCP_UB), Aix-en-Provence (MRS-AIX_UB), Payerne (PAY_UB), Poitiers (POI_UB), Talence (TAL_UB), Turin (TUR_UB), Villanueva Arz (VIL_UB), Zurich (ZUR_UB), Chamonix (CHAM_UV, with UV referring to UB sites in intra-mountainous valleys), and Passy (PAS_UV).
- Ten traffic (TR) sites: Bern (BER_TR), Coimbra (COIM_TR), Madrid Esc. Aguirre (MAD-EA_TR), Milan Senato (MIL-sen_TR), Milan Schivenoglia (MIL-shi_TR), Nice (NIC_TR), Porto (PORT_TR), Roubaix (RBX_TR), Rouen (ROU_TR), and Strasbourg (STG_TR).
- Five industrial (IN) sites: Bailen (BAI_UI, with UI referring to UB-IN environments), Dunkerke-Grande Synthe (DKI_UI), Gijon/Aviles (GIJ_UI), Port de Bouc (PdB_UI), and Gardanne (GAR_SI, with SI referring to sub-urban background industrial environments).
- Seven sub-urban (SUB) sites: Malet (MAL_SUB), Meyreuil (MEY_-SUB), Nogent sur Oise (NGT_SUB), Marnaz (MNZ_SUB), Athens

Demokritos (DEM_SUB), Florence (FLO_SUB), and Florence Montale (MON_SUB).

● Seven rural background (RB) sites: Auchencorth Moss (ACTH_RB), Harwell (HAR_UB), Cwmystwyth (CWM_RB), Detling (DET_RB), Heigham Holmes (HAM_RB), Andra OPE (OPE_RB), Revin (REV_RB).

2.2. Measurements

Measurements of TEs were conducted at the different stations using a variety of approaches (Table S1), including (i) Inductively Coupled Plasma Mass Spectrometry (ICP-MS and ICP-MS-MS) (Glojek et al., 2024), (ii) Proton Induced X-Ray Emission (PIXE) technique (Pio et al., 2020, 2022), and (iii) X-Ray Fluorescence (XRF). Specifically, the most used technique was ICP-MS (39/55 datasets). For ICP-MS analyses, PM samples have to be acid-digested using a combination of acids. While for the TEs regulated in the EU Air quality standards, HF is not required for the sample digestion, for specific TEs, such as Al and Ti, this acid is required to attain bulk dissolution (Querol et al., 2001).

For PIXE analysis (13/55), all elements with atomic number (Z) greater than 10 were directly measured on Teflon© filters using PIXE at a 3 MV Tandetron accelerator with an external beam set-up (Lucarelli et al., 2018). Each sample underwent approximately 5-min irradiation with a 3.2 MeV proton beam (~2 mm^2 spot, 5–50 nA intensity). A filter scanning was conducted to analyze most of the deposit area. PIXE spectra were fitted using the GUPIX code, and elemental concentrations were determined through a calibration curve generated from a set of thin standards with known areal density (Micromatter Inc). When quantifying element concentrations through XRF (4/55), Teflon© filters are also used. Two measuring conditions were fixed to optimize the sensitivity for groups of elements: runs with HV = 15 kV, I = 100 µA, no primary filter, live time = 1000 s, to detect "low Z″ elements (from Na to P), while the "medium-high Z″ elements (from S to Pb) were measured setting HV = 30 kV, I = 500 µA, Ag primary filter (about 50 µm thick), live time = 3000 s (Calzolai et al., 2008).

Typical data quality assurance and quality control (QA/QC) procedures for all these techniques included the regular dispatch and analysis of field-blank filters, the rejection of damaged filters, optimization of the instruments (ICP-MS, PIXE, and XRF) prior to each analysis, regular measurement of filter blanks to ensure appropriate blank subtractions are made from measured values, and setting maximum levels for the standard deviation of the five internal standard-corrected measured intensities of each analysis of each sample. Standard deviations for the final results averaged about 5–10%, but for specific elements, these could be higher, up to about 20%, depending on the analytical tool and concentration levels.

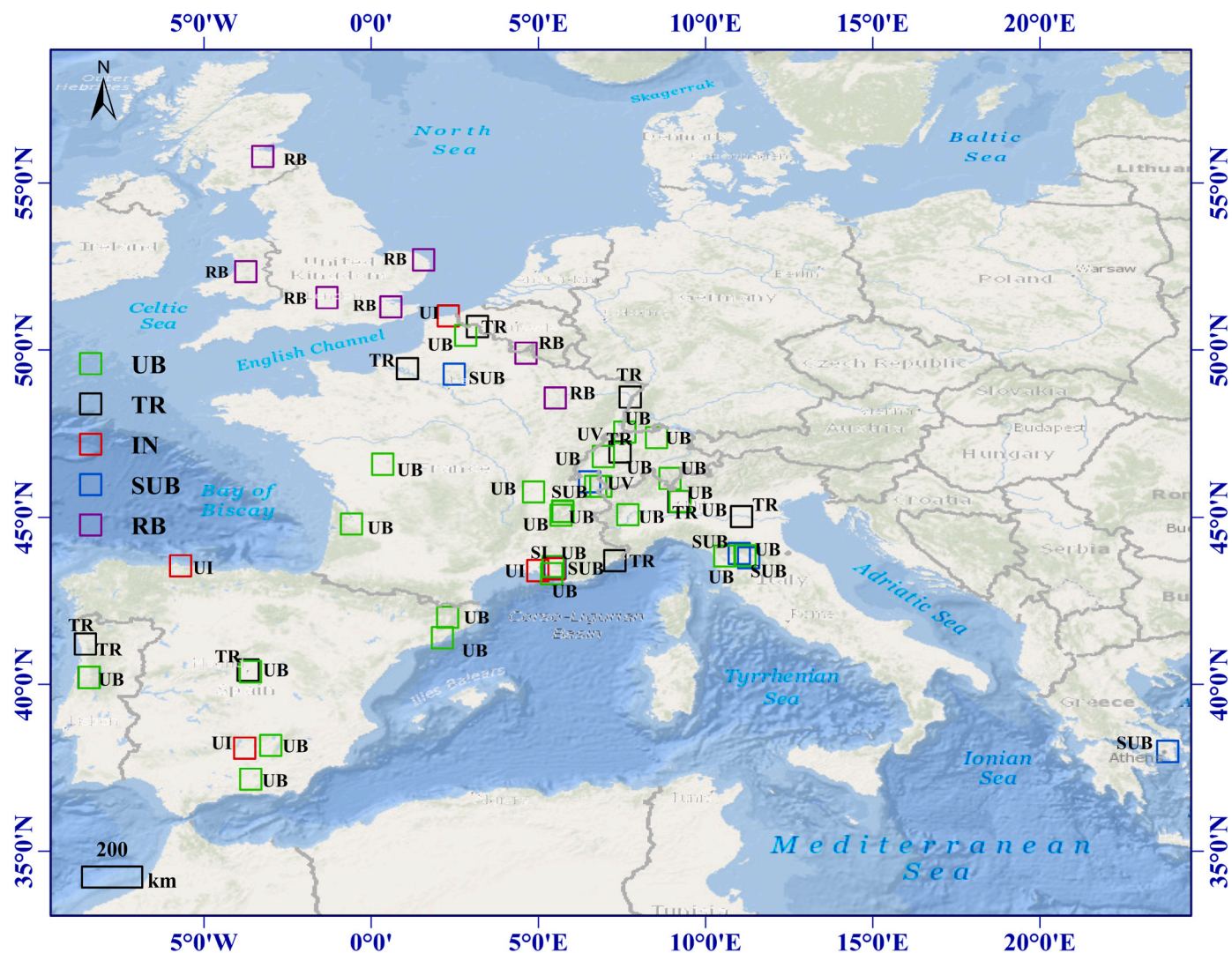Through the compilation of data from 55 monitoring sites, it was

Fig. 1. Location of the sites supplying data on trace elements concentrations for the present study and the type of station. UB/UV, urban background and urban valley; TR, traffic; SUB, sub-urban background; IN, industry (UI, UB-industry; SI, SUB-industry); RB, rural background.

found that the majority of sites monitored a total of 20 TEs. Therefore, for consistency and comparability across all sites, these 20 TEs were selected for detailed analysis in this study. These elements include As, Ba, Br, Cd, Co, Cr, Cu, Hg, Mn, Mo, Ni, Pb, Rb, Se, Sr, Ti, V, Y, Zn, and Zr. Among these, Cd, As, Cr, and Ni can be regarded as carcinogenic elements (WHO, 2007), and the others are classified as non-carcinogenic elements. It is worth mentioning that Sn and Sb were not included because in most sites using PIXE and XRF analyses, these elements were not reported.

2.3. Coefficient of divergence (COD)

Air pollutant data, similar to geospatial data, often exhibit spatial heterogeneity (Yang et al., 2018). To assess the variability in concentrations of ambient pollutants across different monitoring sites, the coefficient of divergence (COD) was utilized (Faridi et al., 2019). The COD_{jk} method quantifies differences between paired sampling sites j and k, defined as:

$$COD_{jk} = \sqrt{\frac{1}{p}\sum_{i=1}^{p}\left(\frac{X_{ij}-X_{ik}}{X_{ij}+X_{ik}}\right)^2} \qquad (Eq.1)$$

where X_{ij} and X_{ik} represent the concentrations of each of the 20 TEs observed at sites j and k respectively, and p is the number of TEs considered. The COD_{jk} values range from 0 to 1: a value approaching 0 indicates similar concentrations between sites, while a value approaching 1 indicates significant differences (Pakbin et al., 2010). The COD_{jk} serves as a relative measure of homogeneity in concentration fields (Liu et al., 2023). Spatially, a low COD_{jk} value (<0.2) suggests high homogeneity between sites, indicating similar pollution levels, whereas a higher COD_{jk} value (>0.2) signifies heterogeneity among sites (Wilson et al., 2005).

In addition, the method of coefficient of variation (COV, *i.e.*, standard deviation divided (STD) by the mean value ($\bar{x}$)) was also used to describe the degree of the spatial variations of TEs concentrations in EU regions, expressed by

$$COV = \frac{STD}{\bar{X}} \qquad (Eq.2)$$

2.4. Self-organizing maps (SOM) analysis

SOM, developed by (Kohonen, 1982, 1997), is a type of artificial neural network that excels in unsupervised learning for clustering (Nakagawa et al., 2020). It can self-organize and assess input patterns while clustering the spatial distribution of functionally similar neurons, ultimately categorizing them. In the present study, SOM was used to identify patterns of TEs in atmospheric samples. Component planes provide an intuitive representation of relationships between variables, where similar gradients indicate positive correlations, and anti-parallel gradients denote negative correlations (Zhu et al., 2020). To enhance visualization, neurons are mapped onto a two-dimensional grid during the self-learning process of the model (Park et al., 2003).

However, there is no universally recommended rule for determining the number of neurons in the output layer. This study adopted the following heuristic equation to select an appropriate neuron count (M): $= 5\sqrt{N}$, where N represents the number of input samples (Vesanto and Alhoniemi, 2000; Zhu et al., 2020). The SOM network model used in this study was constructed using MATLAB software. The input dataset comprised 10 variables, consisting in the concentrations of 10 TEs (As, Ba, Cu, Cd, Cr, Mn, Ti, Zn, Ni, and Pb) across 55 monitoring stations, as these 10 TEs were consistently monitored across all monitoring sites.

2.5. Statistical analysis

The metrics are reported as average concentration (AVE) ± standard

deviation (STD), providing central tendency and dispersion measures across the dataset. The statistically significant differences in TEs concentrations in different seasons and 55 monitoring sites were studied using the Kruskal-Wallis ANOVA on ranks (Kruskal and Wallis, 1952). To further explore significant differences identified by Kruskal-Wallis, Duncan's Multiple Range Test (Duncan, 1955). All statistical analyses were conducted using SPSS Software (IBM SPSS Statistics 25, Chicago, IL, USA), ensuring robustness and reliability in the analysis of complex environmental data. In addition to SPSS, MATLAB (version R2022a, MathWorks, Natick, MA, USA) was employed for SOM analysis.

3. Results and discussion

3.1. Status of TEs data availability and concentrations in Europe

This study conducted an analysis of the annual average concentrations of TEs (Fig. 2a) to enable a comprehensive comparison based on all monitoring sites. Fig. 2a visually illustrated the monitoring period average values of total TEs at each monitoring site, emphasizing substantial obvious difference in total TEs concentrations across seven European countries. The average total concentration of TEs across all monitoring stations was 90 ± 66 (95% CI: 72–108) ng/m^3, displaying a trend similar to that of PM$_{10}$ concentrations, though not exactly the same (Fig. S1).

Differences of TEs concentrations in PM$_{10}$ were also noticeable in different regions and spaces. Specifically, as it could be expected, the concentrations are changing according to the site typologies, with TR and IN (130 ± 66 (95% CI: 88–172) and 131 ± 80 (95% CI: 59–202) ng/m^3) > UB (86 ± 65 (95% CI: 60–111) ng/m^3) > SUB (85 ± 37 (95% CI: 57–112) ng/m^3) > RB (28 ± 13 (95% CI: 16–39) ng/m^3) (Fig. 2 a1). These results suggest that industrial and transportation pollution sources are the primary contributors to TEs in PM$_{10}$. Many studies report that in urban areas brake and tyre wear from vehicles is the main source of a number of TEs, including Cu, Fe, Zn, Sn, Sb, Ba, among others (Amato et al., 2016, among many others). Parviainen et al. (2019) studied TEs pollution in the highly industrialized city of Huelva, Spain, finding that TE concentrations were extremely high within 1 km of industrial parks and gradually decreased with distance. Similarly, Wang et al. (2013) examined the TEs characteristics of PM in Shanghai and also found that the concentration of TEs in PM was higher in industrial areas than in residential areas. Obviously, the industrial contribution to TEs concentrations depends on the type of industries (see Querol et al., 2007). Meanwhile, our results also indicate that most COD_{jk} values between two sites are higher than 0.2, indicating high spatial heterogeneity between these monitoring sites. Further, our results show that the average COD_{jk}s are 0.50 ± 0.16, 0.42 ± 0.10, 0.58 ± 0.17, 0.58 ± 0.18 at UB, TR, IN, and SUB/RB stations, with less dispersion for urban and traffic sites, suggesting more homogeneity across Europe for these types of sites, respectively. As a result, these findings may be useful in identifying the potential sources of TEs and developing common but also site-specific strategies to mitigate its impacts on human health and the environment.

It is worth noting that the intramountainous valleys of CHAM_UV and MNZ_SUB exhibited relatively lower TE concentrations, attributed to the absence of industrial and waste incinerator activities in CHAM_UV, where anthropogenic emissions mainly stem from road traffic, residential heating, and agricultural activities (Brulfert et al., 2006; Weber et al., 2019; Quimbayo-Duarte et al., 2021). Conversely, at MNZ_SUB downstream of Passy, a ventilation zone formed due to a jet-like structure at the valley exit (Quimbayo-Duarte et al., 2021), significantly reducing TE and PM$_{10}$ levels, with emissions concentrated within this zone.

Data gathered from UB sites evidenced elevated levels of TEs in Italy, Spain and Portugal, with average concentrations of the sum of the TEs in PM$_{10}$ in the range 155–165 ng/m^3 (Fig. 2 a2). Moreover, the pattern observed in TEs concentrations aligned with the trend seen in PM$_{10}$
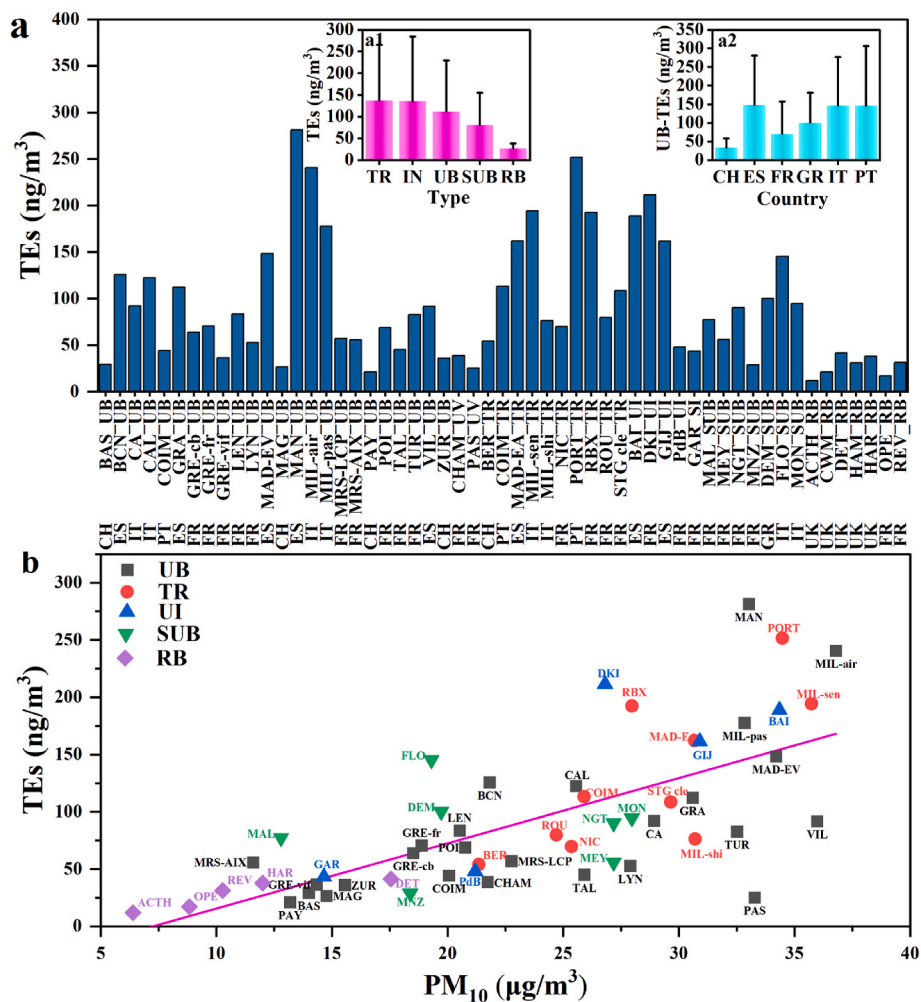
Fig. 2. Average total trace elements (a) concentrations of the European datasets compiled in this study, and PM$_{10}$/TEs cross correlation plot (b). (a1) Idem but for different environments. (a2) Idem but for different UB in the various countries.

concentrations across all countries but not in all cases (Fig. S1). Thus, Fig. 2b displays the cross-correlation of the sum of TEs with the corresponding PM$_{10}$ concentrations. The results indicate that at PAS_UB, VIL_UB, TUR_UB, LYN_UB, and TAL_UB, as well as MIL-shi_TR, NIC_TR, PdB_UI, MEY_SUB, relatively high PM$_{10}$ concentrations contain relatively lower concentrations of TEs. Conversely, at MAN_UB, MIL-air_UB, PORT_TR, RBX_TR, FLO_SUB, and MAL_SUB, relatively lower of concentrations of PM$_{10}$ contain relatively higher concentrations of TEs. Such results clearly indicate the role of various sources (like marine emissions or domestic biomass burning) at modulating the PM mass but not the TE concentrations.

3.2. Seasonal variations

Since the concentrations of TEs varies largely with the type of monitoring site (see panels in Fig. 2a), the seasonal variations of the TEs studied are further discussed based on the site classification. The seasonal TEs patterns (Spring: March to May, Summer: June to August, Autumn: September to November, and Winter: December to February) were evaluated for different types of sites, all sites together, and also separately for each monitoring site using ANOVA on ranks with Dunn's method (Fig. 3 and S2). Significant seasonal differences ($p < 0.05$) in total TEs concentrations were observed across different types of sites, including UB, TR, IN, SUB, and RB. Specifically, UB, TR, and SUB sites showed a trend of lower concentrations in Summer compared to Spring, Autumn, and Winter. In contrast, IN areas exhibited a distinctive trend

of lower concentrations in Autumn compared to Summer, Spring, and Winter. In RB sites, TEs concentrations were lowest in Winter and highest in spring. These variations are likely influenced by factors such as regional sources of pollution and meteorological conditions, with industrial areas particularly affected by seasonal changes in specific industrial activities (In'T Veld et al., 2021). Such anthropogenic and meteorological variations also contributed to differences in the observed trends when analyzing the seasonal variations at individual monitoring sites (Fig. S2).

The study conducted by Mrazovac Kurilić et al., 2020 revealed severe heavy metal pollution in PM$_{2.5}$ during autumn and winter in Guangzhou, China, aligning with the temporal variation of PM$_{2.5}$ concentration. Similarly, Galon-Negru et al. (2019) observed distinct seasonal variations in the water-soluble concentrations of heavy metals (Al, Fe, Zn, As, Cr, Pb) in PM$_{2.5}$ in Iasi, northeastern Romania, with higher concentrations in the cold season and lower concentrations in the warm season. Additionally, Hernández-Pellón and Fernández-Olmo (2019) measured PM$_{10}$ in the Cantabria region, northern Spain, highlighting the highest concentrations of Mn, Fe, Zn, and Pb in autumn, associated with the manganese alloy industry, and increased deposition rates in winter and autumn, correlating with elevated monthly precipitation. Also, Glojek et al. (2024) observed larger concentrations in winter than in summer for Mn, Fe, Cd, and Zn in an Alpine valley in Slovenia influenced by emissions from a large cement plant. Observing these seasonal trends is crucial for a comprehensive understanding of TE behaviour under diverse temporal and environmental conditions, providing robust
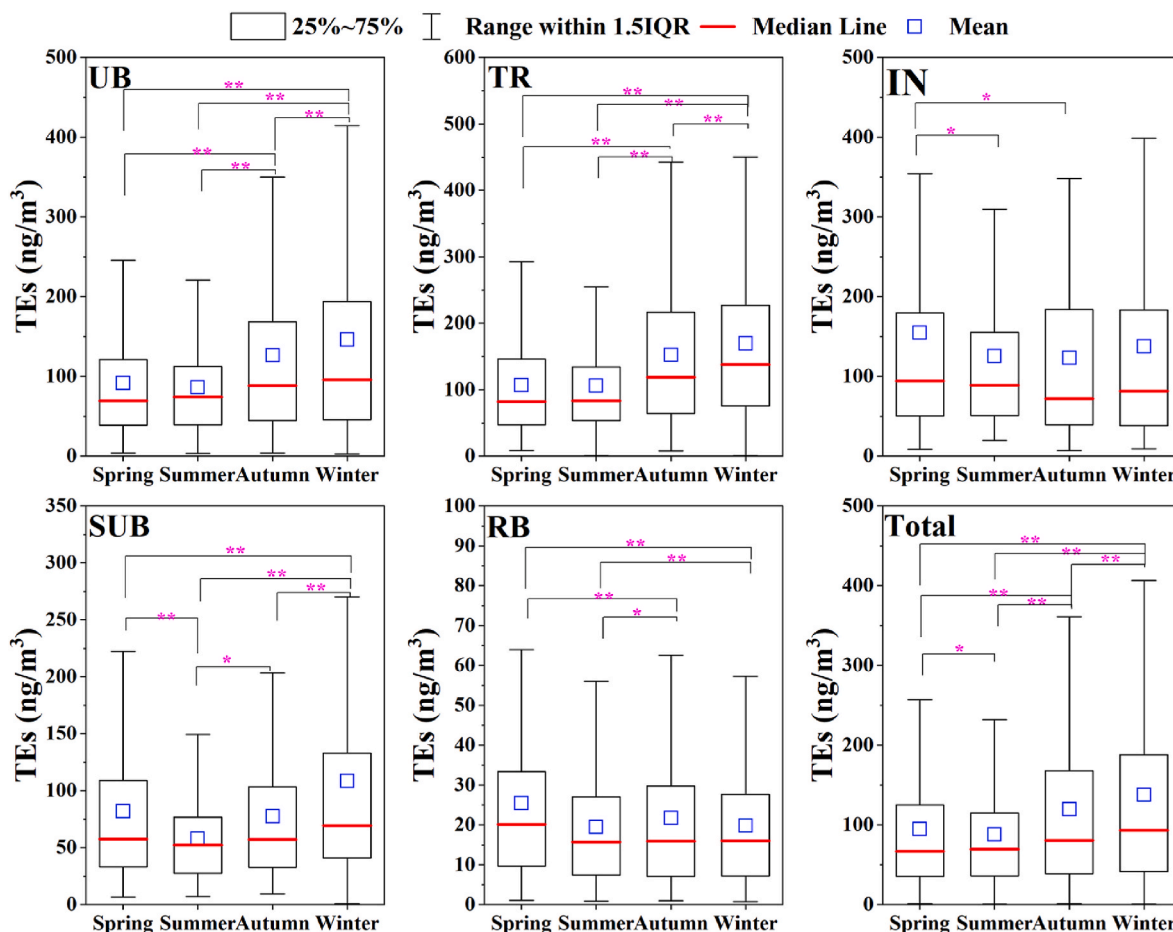
Fig. 3. Seasonal variability in total trace elements (TEs) concentrations across different environments. *, $p < 0.05$; **, $p < 0.01$. Note the different scales for the different typology of sites.

support for environmental monitoring, management, and pollution control strategies. Furthermore, COD results indicate significant temporal heterogeneity among monitoring sites, with COD_{jk} greater than 0.2 during winter and summer at 47 out of 55 sites, followed by spring-winter seasons (40/55) and summer-autumn seasons (35/55), implying distinct emission sources among the seasons (Fig. S3). Therefore, different control measures, if necessary, are prone to be performed varying with seasonal periods.

3.3. Concentrations of individual TEs

Given the absence of specified concentration limits/targets for TEs in ambient air in EU, except for As (6 ng/m³), Pb (500 ng/m³), Cd (5 ng/m³), and Ni (20 ng/m³) as outlined by the EU (2004, 2008), this study compiled and compared the concentration ranges of 20 TEs across seven countries. Fig. 4 illustrates the numerical concentration ranges for each TE, revealing that the average concentrations of As, Pb, Cd, and Ni all
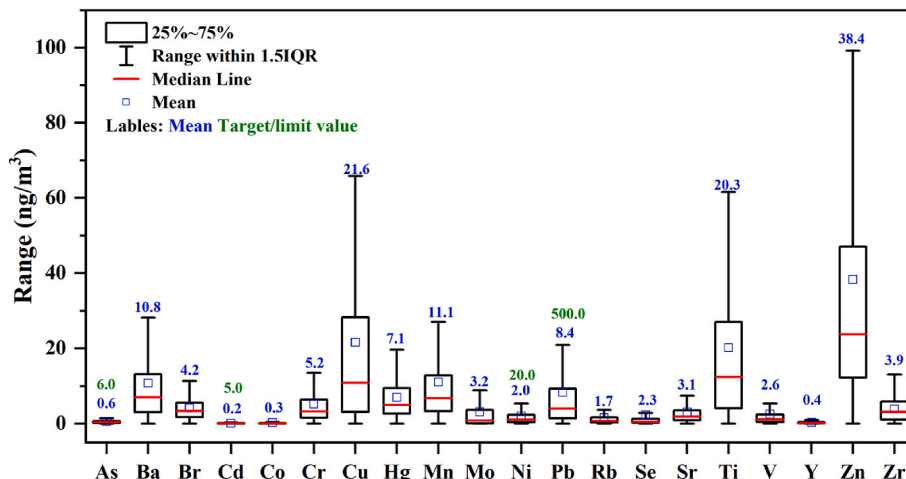
Fig. 4. Range of different trace elements in PM₁₀ among the European countries.

6

comply with EU standards. The highest concentrations were recorded for Zn, Cu and Ti (40, 23, and 20 ng/m³), followed by Mn and Ba (12 and 11 ng/m³), all TEs being conventionally attributed to brake-wear, tyre-wear and road dust resuspension in urban environments (Amato et al., 2016; Charron et al., 2019; Rahman et al., 2021). Inhalation of these TEs poses significant health risks. For instance, As, Pb, Cd, and Ni are known carcinogens, with exposure linked to lung and bladder cancers (Wu et al., 2022; Wang et al., 2023). Zn, Cu, and Mn, while essential

Fig. 5. Frequency distribution and Coefficient of variation (COV) of 20 trace elements (TEs) for all monitoring sites in Europe.

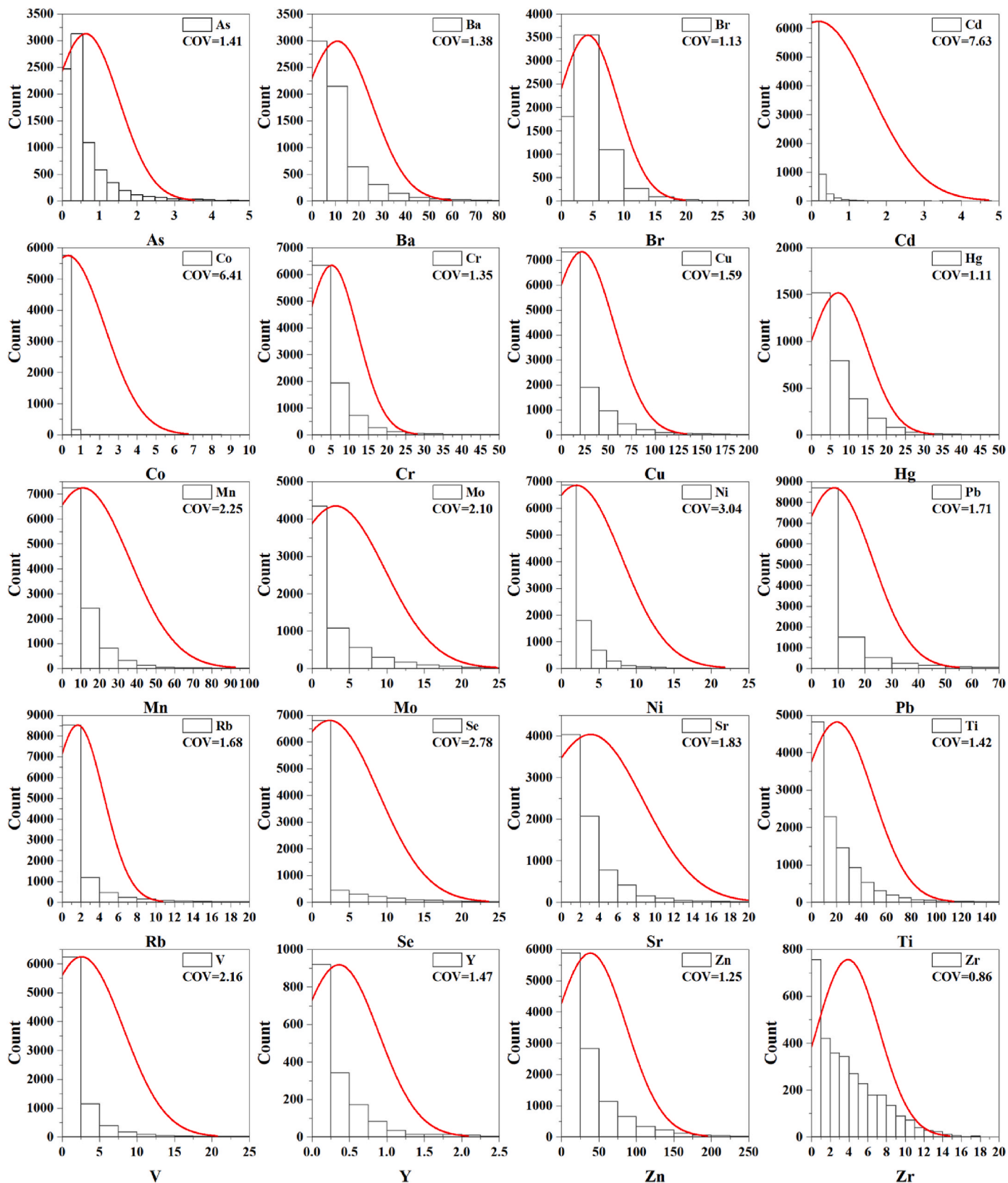in small amounts, can cause toxicity at higher concentrations, leading to respiratory and cardiovascular problems (Wu et al., 2019). Overall, the presence of these toxic metals in PM highlights the need for stricter regulatory measures and continuous monitoring to mitigate adverse health effects on urban populations.

Fig. 5 displays the frequency distribution and COV of concentrations for these 20 TEs at all monitoring sites. While these TEs concentrations generally follow a normal distribution, their COVs are all greater than 1, indicating significant spatial disparities among the TEs across Europe, potentially influenced by spatial factors. Particularly, Cd exhibits the highest COV (7.65), suggesting the greatest variability of this element among different monitoring sites, possibly influenced by a greater array of spatial factors. Similarly, the average concentrations of each TE has been compiled for the different types of sites (Table S2), providing a more comprehensive dataset to guide future environmental protection policies.

Additionally, the analysis of concentrations for these 20 TEs in PM_{10} revealed varying proportions of non-carcinogenic and carcinogenic metals across different environments (Fig. 6) and each monitoring site (Fig. S4). TEs were classified into two groups: non-carcinogenic and carcinogenic elements (WHO, 2007). The distribution showed a range of 84%–99% for non-carcinogenic TEs and 1%–16% for carcinogenic TEs. Notably, among all sites, Zn, Cu, and Ti dominated among non-carcinogenic TEs, constituting 29% ± 9%, 16% ± 7%, and 14% ± 8%, respectively. Subsequent contributors included Ba, Mn, Pb and Mo, accounting for 9% ± 6%, 9% ± 6%, 6% ± 3%, and 2% ± 3%,

respectively. For carcinogenic TEs, Cr and Ni exhibited higher proportions, comprising 3% ± 1% and 2% ± 2%, respectively, all exceeding 2%. These trends remained consistent across environmental settings and countries, with Zn, Ti, and Cu prominent among non-carcinogenic TEs, Cr and Ni predominated among carcinogenic TEs (Figs. S4–S5). Specifically, in different environmental categories, the highest average concentrations were observed for Zn in IN and TR (46 ± 24 and 44 ± 27 ng/m³, respectively), Cu in TR (30 ± 11 ng/m³), Mn in IN (29 ± 36 ng/m³), Ti in IN (20 ± 17 ng/m³), Ba in TR (18 ± 9 ng/m³), Pb in TR (9 ± 7 ng/m³), and Cr in IN (6 ± 3 ng/m³). Concerning different countries, the maximum average concentrations were found for Zn in Portugal (54 ± 40 ng/m³), Ti, Cu, and Pb in Spain (33 ± 11, 28 ± 29, 10 ± 10 ng/m³, respectively), and Cr and Ni in Italy (5 ± 2 and 4 ± 5 ng/m³), respectively. Additionally, at five RB monitoring sites in the UK, although the overall concentrations of TEs were relatively low, the proportion of carcinogenic elements was relatively high, ranging from 8% to 15%.

Nevertheless, these values were generally lower than those reported in China (Wang et al., 2013; Cheng et al., 2018; Jiang et al., 2019), South Korea (Roy et al., 2019), and India (Jena and Singh, 2017). In addition, the concentrations of these TEs at sites in Spain (UB, IND, TR, RB) decreased by approximately one order of magnitude compared to the study by Querol et al. (2007) concerning TEs concentrations in PM_{10} from 1995 to 2006, a decrease which can be mainly attributed to the implementation of industrial emission directives and the elimination of lead in gasoline. Spatially, between 1990 and 2021, Cu emissions in the EU-27 increased 4% according to EEA (2023b). The primary sources of
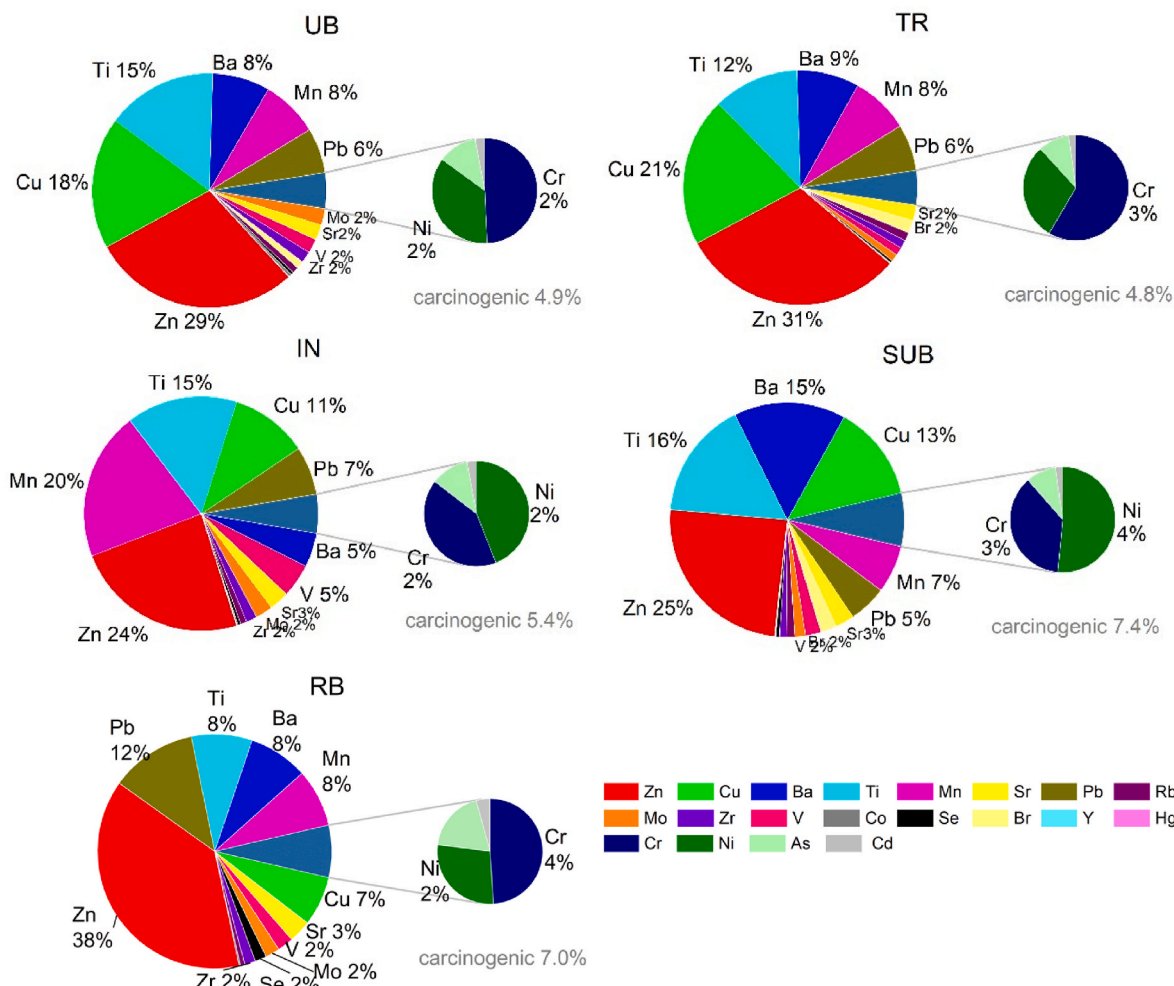

Fig. 6. Proportion of different trace elements varies among different environments. Elements with mass proportions lower than 1.5% are not displayed, and the mass proportion of carcinogenic elements (Cr, Ni, As, and Cd) are given below the smaller pie charts.

these emissions are attributed to automobile tyre and brake wear, as well as industrial emissions, as indicated by EEA (2018).

Many previous studies outlined the contributions of various emission sources to TEs atmospheric concentrations. Industrial processes were identified as the main contributors to As, Cd, Cu, Pb, Mn, and Zn (Allen et al., 2001; Marcazzan et al., 2001; Querol et al., 2007; Fernández-Camacho et al., 2012; Rodriguez-Espinosa et al., 2017). Ni and V were predominantly associated with oil combustion (Nriagu and Pacyna, 1988; Querol et al., 2007; Fernández-Camacho et al., 2012), while Cr was mainly associated with coal combustion and stainless-steel production (Pyle et al., 2001; Gao et al., 2002; Querol et al., 2007). Metal industry operations were dominant sources for Mn, Zn, As, Pb, Co, and Cr (Querol et al., 2007; Fernández-Camacho et al., 2012; Pokorná et al., 2016). Additionally, soils and re-suspended dust played a significant role in Mn, Ni, V, Cu, and Ti emissions (Querol et al., 2007; Amato et al., 2009, 2016; Pant and Harrison, 2013; Squizzato et al., 2017). Municipal solid waste incinerators were major contributors to As, Cd, Cr, Cu, Hg, Pb, Mn, Ni, and V levels (Font et al., 2015; Ziegler et al., 2021). Vehicle exhaust emerged as the primary source for TEs, including Cr, Pb, Cu, Zn, Cd, and Ba (Sternbeck et al., 2002; Schauer et al., 2006; Querol et al., 2007; Squizzato et al., 2017; Charron et al., 2019; Koc et al., 2023). Therefore, understanding the diverse sources and distribution patterns of TEs in particulate matter is essential for developing effective environmental management strategies. For instance, at the DKI_UI site, Mn and Zn accounted over 70% of the total ETs, indicating the need to prioritize control measures for nearby industrial emissions. Hence, the dominance of specific TEs in various regions emphasizes the need for targeted mitigation efforts tailored to the unique pollution profiles of different areas. Specific source apportionment work will be addressed in the subsequent article, where detailed analyses and investigations into the origins of these TEs will be conducted.

3.4. SOM analysis

The correlation among elements can effectively indicate common sources or pathways of PM deposition and is widely used in TEs database analysis (Huang et al., 2009; Ramos-Miras et al., 2011). Initially, we selected for SOM analysis 10 TEs (As, Ba, Cu, Cd, Cr, Mn, Ti, Zn, Ni, Pb) that were co-consistently monitored across 55 sites, a study including both annual SOM analysis (Fig. 7) and seasonal SOM analysis (Fig. S7). SOM maps in Fig. 7 illustrated the spatial relationships among these 10 TEs across 55 monitoring sites. Each SOM matrix represented the index values obtained after dimension reduction, indicated by a gradient ranging from black (low values) to yellow (high values). By comparing the color gradients on the SOM, one could visually observe the qualitative relationships among the 10 TEs in different geographical locations. Overall, these TEs exhibited visible spatial variations, indicating that their emissions were primarily influenced by local sources and different types of origins. Additionally, at specific positions on certain SOMs, certain elements displayed similar brightness, signifying robust positive correlations among them. For instance, at the MAN_UB site, Cd, Cu, and Pb exhibited analogous color gradients, suggesting substantial positive correlations among these TEs. Similarly, the SOMs for the 10 TEs in different seasons (Fig. S7) displayed varying degrees of correlations. For instance, at the DKI_UI site, in spring, there was correlation among As, Cd, Mn, Ni, and Zn, while in summer, there was correlation among Mn and Zn. In autumn and winter, at the MAN_UB site, there was correlation among Cd, Cu, Pb, and Zn. This suggested the potential existence of common sources for these elements, which can be further verified by correlation analysis.
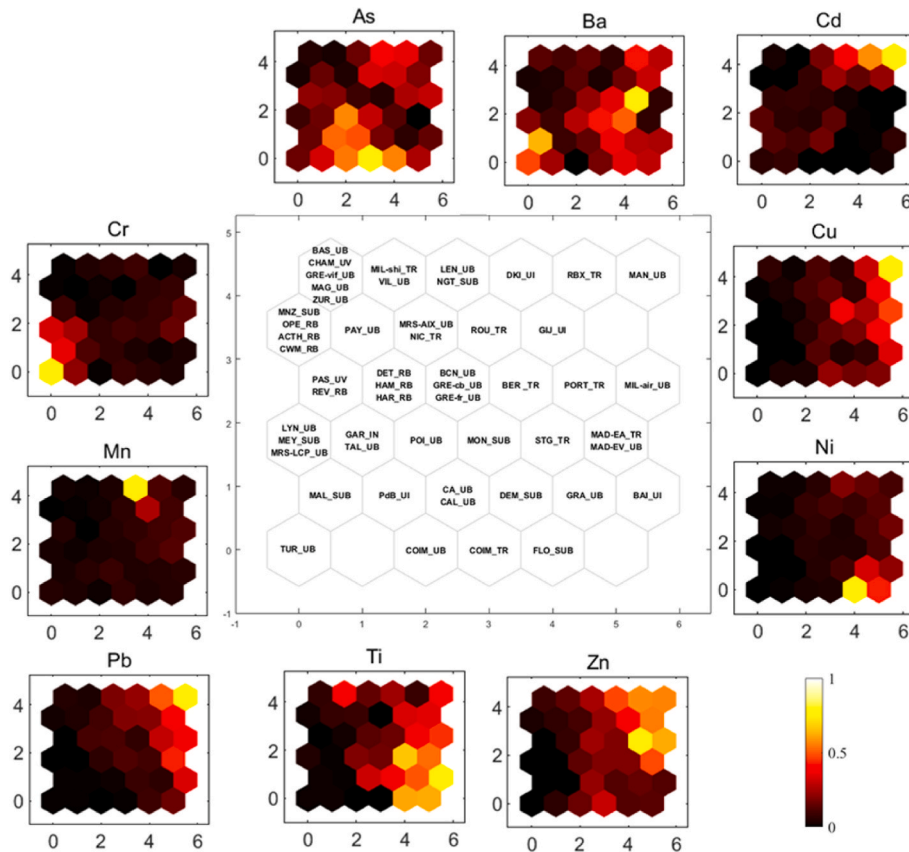

Fig. 7. Total SOM matrix map of the 10 trace elements across 55 sites. The color gradient from dark to light represents the concentration of elements, with darker shades indicating lower concentrations and yellow representing higher concentrations.

3.5. Correlation analysis

To verify the SOM calculation results, this study conducted Pearson correlation analysis on all TEs in PM_{10} varying with locations (Fig. 8) and seasons (Figs. S7–S10). Fig. 8 shows the correlations of TEs at different locations, revealing distinct correlation patterns across various

sites. In general, robust positive correlations among TEs suggest shared geochemical characteristics or origins, with marker elements playing a role in identifying potential sources (Zhong et al., 2016). In this study, the correlation patterns of various TEs demonstrate varying degrees of significance depending on the type of location. For instance, in UB sites, notable correlations such as Cr vs. Hg ($r = 0.67$), Cu vs. Pb ($r = 0.73$),
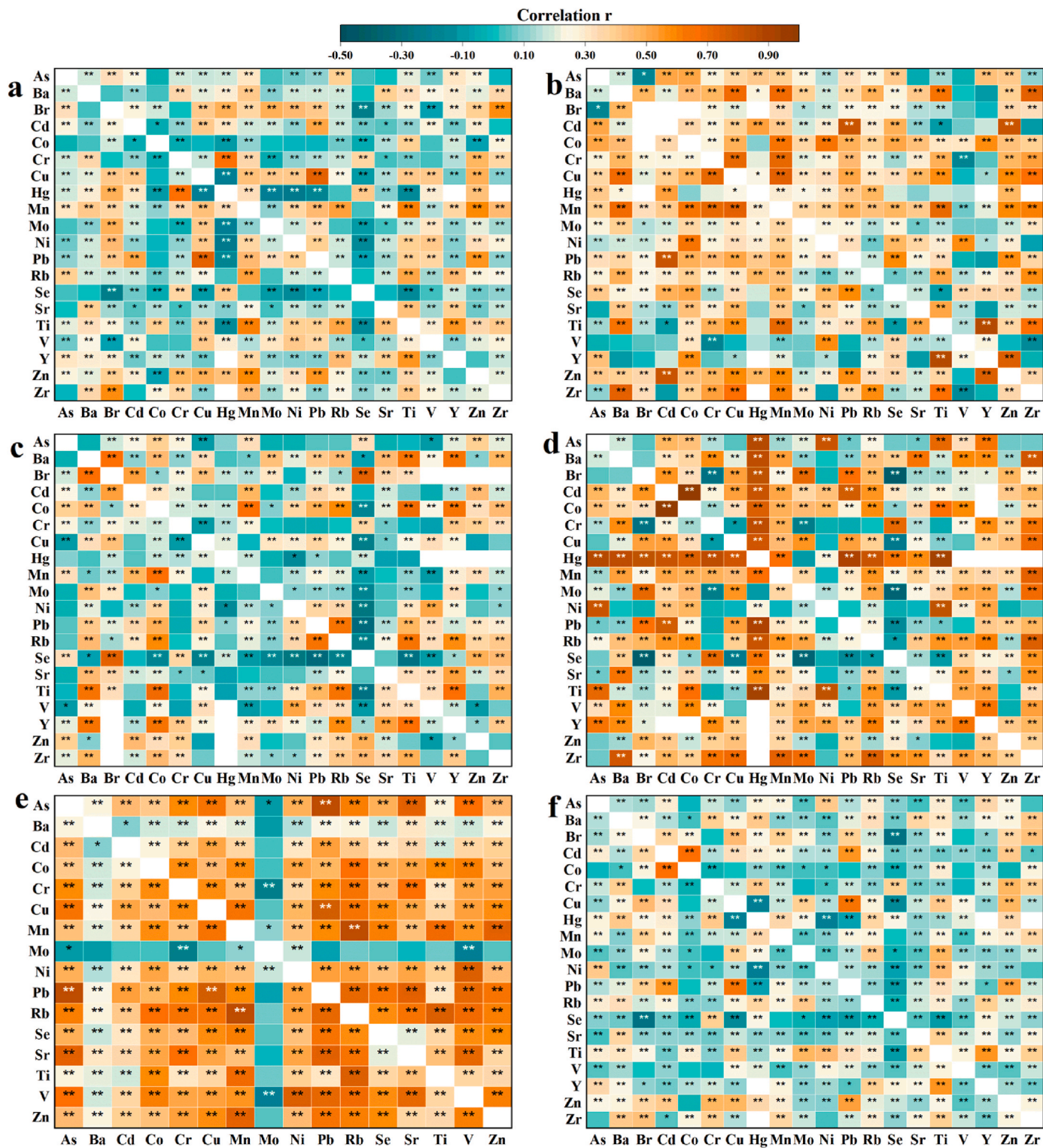

Fig. 8. Correlations among trace elements in different environments including a, urban background; b, traffic; c, industry; d, suburban; e, rural background; and f, total data. (The lack of monitoring data for elements Br, Hg, Y, and Zr at rural background sites results in the exclusion of these elements from the elemental correlations analysis in e.)

and Mn vs. Ti (r = 0.62) were observed, indicating shared pollution sources in urban environments. This finding corroborates and reinforces the results obtained from the SOM analysis. TR sites exhibited significant correlations among multiple elements, including Ba vs. Zr, Ti, Mn, and Cu (r > 0.6), Cd vs. Zn and Pb (r > 0.8), and Cr vs. Cu and Mn (r > 0.7), highlighting the substantial impact of traffic emissions on these element relationships. IN sites displayed significant associations among elements like Ba with Ti, Br, Se (r > 0.6), and Co with Y, Ti, Mn (r > 0.6), reflecting the influence of industrial activities on these element relationships.

In SUB sites, there was a stronger correlation among various TEs, including As, Ba, Br, Cr, Cu, Hg, suggesting a relatively similar pollution source. In the study of TE correlations in RB sites, significant associations were found, for instance, As vs. Pb, Mn, and Co, possibly originating from a common pollution source. Additionally, Br showed significant correlations with Se, Pb, Cu, and Cd, possibly influenced by agricultural activities or other natural factors. The correlation of Co with multiple elements reflected complex interactions among these elements in rural areas, likely influenced by coal combustion, agricultural activities and other environmental factors. The associations between Cr, Cu, Hg, and Mn also suggest the joint influence of agricultural activities and natural factors in rural environments. Furthermore, the correlations between Pb, and Se underscore the potential impact of soil and water on the relationships among these elements in rural background sites.

The strength of correlations among elements in different environments varied with the seasons (Figs. S7–S10). For example, at UB sites, the correlation between Ba and Sr was highest in summer (r = 0.70), while in winter it was only 0.28. Similarly, Br vs. Zr showed correlations greater than 0.60 in both summer and winter, whereas in spring and autumn, it was below 0.50. Likewise, at TR sites, the correlation between Cr and Pb was higher in autumn and winter than in spring and summer, possibly due to lower temperatures promoting emissions from traffic and other sources during the colder seasons (Hwang et al., 2018), or lower mixing depths concentrating local emissions. At IN sites, the correlation between Co and Mn reached 0.87 in spring, while in other seasons, it was below 0.52. At SUB and RB sites, where sources are relatively similar, correlations among elements also varied to different extents with the seasons. Notably, the highest correlations were observed in RB sites, despite lower concentrations, which may be primarily due to similar meteorological influences in rural areas. The variation in the concentration of TEs was significant due to the specific meteorological conditions at each site, land use patterns, and various anthropogenic activities which implied that every different location has its own characteristic TE composition (Mondal and Singh, 2021). Detailed seasonal correlation analysis can be found in Figs. S7–S10.

3.6. Environmental implications and limitations

The findings of this study hold significant implications for environmental management and policy development concerning TEs in PM_{10} across urban Europe. The dominance of non-carcinogenic metals such as Zn, Ti, and Cu highlights the diverse sources contributing to urban air pollution. This underscores the urgent need for stricter emissions controls targeting industrial and traffic-related activities to mitigate environmental impacts. However, the study also acknowledges limitations, including the high spatial heterogeneity observed among monitoring sites, which suggests the influence of localized factors not fully captured in the current research framework. Future studies should address these limitations by integrating advanced spatial modeling techniques and conducting more detailed source apportionment analyses to enhance the accuracy of environmental assessments and inform targeted mitigation strategies. Moreover, our study stops short of directly linking the findings to health outcomes. Future research could address these gaps by conducting more detailed epidemiological assessments and exploring the specific health impacts of TE exposure in urban environments.

4. Conclusions and outlook

This study presents a comprehensive assessment of concentrations for 20 trace elements (TEs) in PM_{10} at 55 monitoring sites in seven European countries (Switzerland, Spain, France, Greece, Italy, Portugal, UK) over a decade (2013–2022). Measurement campaigns were performed at 26 urban background (UB), ten traffic (TR), five industrial (IN), seven suburban (SUB), and seven rural background (RB) sites. The annual concentrations of the sum of the 20 TEs varied across urban Europe, within the range of 12–281 ng/m^3, indicating the varied pollution situations across Europe. In terms of location type, TR and IN sites had the highest concentrations (130 ± 66 and 131 ± 80 ng/m^3), followed by UB, SUB, and RB sites (86 ± 65, 85 ± 37, 28 ± 13 ng/m^3, respectively) indicating that industrial, traffic, and other urban sources were primary contributors to TEs. Meanwhile, our results show that the average $COD_{jk}s$ were higher than 0.2 at UB, TR, IN, and SUB/RB stations, indicating the high spatial heterogeneity between these monitoring sites. The seasonal variability in total TEs showed significant differences ($p < 0.05$) at different types of sites, which may be caused by factors such as regional sources of pollution and meteorological conditions.

Moreover, the examination of the weights of TEs in PM_{10} across diverse environments highlighted clear distinctions in the proportions of non-carcinogenic and carcinogenic metals, with Zn, Ti and Cu dominating among non-carcinogenic TEs, and Cr and Ni being prominent among carcinogenic TEs. These patterns remained consistent across various environmental categories and countries, with specific TE concentrations peaking in specific environments.

Using SOM analysis for the 10 shared TEs across all sites, along with correlation analyses conducted on 20 TEs across diverse locations and seasons, unveiled specific correlations among TEs, emphasizing the impact of traffic emissions, industrial activities, and natural factors on element relationships. In essence, this observation highlights the existence of TEs in the environment and furnishes a more extensive dataset for informing future environmental protection policies. In our continued investigation of these datasets, we will concentrate on source apportionment analysis and epidemiological assessments to understand associations between TEs, their sources and health implications (if any).

In summary, this study provides crucial insights into the spatial and temporal patterns of TEs in the European atmosphere, supplying vital information to inform environmental policies and interventions. Proposed measures encompass advocating for stricter emission controls, promoting exposure reduction, and enhancing public awareness to combat air pollution's harmful impacts on both public health and the environment. However, continuous monitoring and research efforts are essential for effectively mitigating these adverse effects.

CRediT authorship contribution statement

Xiansheng Liu: Writing – original draft, Methodology, Data curation, Conceptualization. **Xun Zhang:** Methodology, Formal analysis. **Tao Wang:** Writing – original draft, Software, Methodology, Formal analysis. **Bowen Jin:** Data curation. **Lijie Wu:** Methodology. **Rosa Lara:** Methodology. **Marta Monge:** Project administration. **Cristina Reche:** Data curation. **Jean-Luc Jaffrezo:** Writing – review & editing, Data curation. **Gaelle Uzu:** Writing – review & editing, Data curation. **Pamela Dominutti:** Data curation. **Sophie Darfeuil:** Data curation. **Olivier Favez:** Data curation. **Sébastien Conil:** Data curation. **Nicolas Marchand:** Data curation. **Sonia Castillo:** Data curation. **Jesús D. de la Rosa:** Data curation. **Grange Stuart:** Data curation. **Konstantinos Eleftheriadis:** Data curation. **Evangelia Diapouli:** Data curation. **Maria I. Gini:** Data curation. **Silvia Nava:** Data curation. **Célia Alves:** Data curation. **Xianxia Wang:** Formal analysis. **Yiming Xu:** Formal analysis. **David C. Green:** Data curation. **David C.S. Beddows:** Data curation. **Roy M. Harrison:** Data curation. **Andrés Alastuey:** Writing – review & editing. **Xavier Querol:** Writing – review & editing,

Supervision, Funding acquisition, Data curation, Conceptualization.

Declaration of competing interest

The authors declare that they have no known competing financial interests or personal relationships that could have appeared to influence the work reported in this paper.

Data availability

Data will be made available on request.

Acknowledgements

Appendix A. Supplementary data

Supplementary data to this article can be found online at https://doi.org/10.1016/j.envres.2024.119630.

References

Abbasi-Kangevari, M., Malekpour, M., Masinaei, M., Moghaddam, S.S., Ghamari, S., Abbasi-Kangevari, Z., Rezaei, N., Rezaei, N., Mokdad, A.H., Naghavi, M., 2023. Effect of air pollution on disease burden, mortality, and life expectancy in North Africa and the Middle East: a systematic analysis for the global burden of disease study 2019. Lancet Planet. Health 7, e358–e369.

Aksu, A., 2015. Sources of metal pollution in the urban atmosphere (A case study: tuzla, Istanbul). J Environ Health Sci Eng 13, 1–10.

Allen, A.G., Nemitz, E., Shi, J.P., Harrison, R.M., Greenwood, J.C., 2001. Size distributions of trace metals in atmospheric aerosols in the United Kingdom. Atmos. Environ. 35, 4581–4591 (1994).

Amato, F., Escrig, A., Sanfelix, V., Celades, I., Reche, C., Monfort, E., Querol, X., 2016. Effects of water and CMA in mitigating industrial road dust resuspension. Atmos. Environ. 131, 334–340 (1994).

Amato, F., Pandolfi, M., Viana, M., Querol, X., Alastuey, A., Moreno, T., 2009. Spatial and chemical patterns of PM10 in road dust deposited in urban environment. Atmos. Environ. 43, 1650–1659 (1994).

Baulig, A., Singh, S., Marchand, A., Schins, R., Barouki, R., Garlatti, M., Marano, F., Baeza-Squiban, A., 2009. Role of Paris PM2. 5 components in the pro-inflammatory response induced in airway epithelial cells. Toxicology 261, 126–135.

Borsi, S.H., Goudarzi, G., Sarizadeh, G., Dastoorpoor, M., Geravandi, S., Shahriyari, H.A., Akhlagh Mohammadi, Z., Mohammadi, M.J., 2022. Health endpoint of exposure to criteria air pollutants in ambient air of of a populated in Ahvaz City, Iran. Front. Public Health 10, 869656.

Briffa, J., Sinagra, E., Blundell, R., 2020. Heavy metal pollution in the environment and their toxicological effects on humans. Heliyon 6, e04691.

Brulfert, G., Chemel, C., Chaxel, E., Chollet, J., Jouve, B., Villard, H., 2006. Assessment of 2010 air quality in two Alpine valleys from modelling: weather type and emission scenarios. Atmos. Environ. 40, 7893–7907 (1994).

Budi, H.S., Catalan Opulencia, M.J., Afra, A., Abdelbasset, W.K., Abdullaev, D., Majdi, A., Taherian, M., Ekrami, H.A., Mohammadi, M.J., 2024. Source, toxicity and carcinogenic health risk assessment of heavy metals. Rev. Environ. Health 39, 77–90.

Calzolai, G., Chiari, M., Lucarelli, F., Mazzei, F., Nava, S., Prati, P., Valli, G., Vecchi, R., 2008. PIXE and XRF analysis of particulate matter samples: an inter-laboratory comparison. Nucl. Instrum. Methods Phys. Res. Sect. B Beam Interact. Mater. Atoms 266, 2401–2404.

Chalvatzaki, E., Chatoutsidou, S.E., Lehtomäki, H., Almeida, S.M., Eleftheriadis, K., Hänninen, O., Lazaridis, M., 2019. Characterization of human health risks from particulate air pollution in selected European cities. Atmosphere 10, 96.

Charron, A., Polo-Rehn, L., Besombes, J., Golly, B., Buisson, C., Chanut, H., Marchand, N., Guillaud, G., Jaffrezo, J., 2019. Identification and quantification of particulate tracers of exhaust and non-exhaust vehicle emissions. Atmos. Chem. Phys. 19, 5187–5207.

Chen, L., Maciejczyk, P., Thurston, G.D., 2022. Metals and air pollution. In: Handbook on the Toxicology of Metals. Elsevier, pp. 137–182.

Cheng, X., Huang, Y., Zhang, S., Ni, S., Long, Z., 2018. Characteristics, sources, and health risk assessment of trace elements in PM10 at an urban site in Chengdu, Southwest China. Aerosol Air Qual. Res. 18, 357–370.

Collin, M.S., Venkatraman, S.K., Vijayakumar, N., Kanimozhi, V., Arbaaz, S.M., Stacey, R.S., Anusha, J., Choudhary, R., Lvov, V., Tovar, G.I., 2022. Bioaccumulation of lead (Pb) and its effects on human: a review. Journal of Hazardous Materials Advances 7, 100094.

Coudon, T., Hourani, H., Nguyen, C., Faure, E., Mancini, F.R., Fervers, B., Salizzoni, P., 2018. Assessment of long-term exposure to airborne dioxin and cadmium concentrations in the Lyon metropolitan area (France). Environ. Int. 111, 177–190.

Duncan, D.B., 1955. Multiple range and multiple F tests. Biometrics 11, 1–42.

EEA, 2018. EEA air quality Statistics. https://www.eea.europa.eu/data-and-maps/dashboards/air-quality-statistics.

EEA, 2023a. Europe's air quality status 2023 Briefing no. 05/2023. https://www.eea.europa.eu/publications/europes-air-quality-status-2023.

EEA, 2023b. EEA European union emission inventory report 1990–2021 report No 4/2023. https://www.eea.europa.eu/publications/european-union-emissions-inventory-report-1990-2021.

EU, 2004. Directive 2004/107/EC of the European Parliament and of the Council of 15 December 2004 relating to arsenic, cadmium, mercury, nickel and polycyclic aromatic hydrocarbons in ambient air. From the Official Journal of the European Communities 26, 2005.

EU, 2008. Directive 2008/50/EC of the European Parliament and of the Council of 21 May 2008 on ambient air quality and cleaner air for Europe. Off. J. Eur. Union.

Faraji Ghasemi, F., Dobaradaran, S., Saeedi, R., Nabipour, I., Nazmara, S., Ranjbar Vakil Abadi, D., Arfaeinia, H., Ramavandi, B., Spitz, J., Mohammadi, M.J., 2020. Levels and ecological and health risk assessment of PM 2.5-bound heavy metals in the northern part of the Persian Gulf. Environ. Sci. Pollut. Res. Int. 27, 5305–5313.

Faridi, S., Niazi, S., Yousefian, F., Azimi, F., Pasalari, H., Momeniha, F., Mokammel, A., Gholampour, A., Hassanvand, M.S., Naddafi, K., 2019. Spatial homogeneity and heterogeneity of ambient air pollutants in Tehran. Sci. Total Environ. 697, 134123.

Fernández-Camacho, R., Rodríguez, S., De la Rosa, J., de la Campa, A.S., Alastuey, A., Querol, X., González-Castanedo, Y., Garcia-Orellana, I., Nava, S., 2012. Ultrafine particle and fine trace metal (As, Cd, Cu, Pb and Zn) pollution episodes induced by industrial emissions in Huelva, SW Spain. Atmos. Environ. 61, 507–517 (1994).

Font, A., de Hoogh, K., Leal-Sanchez, M., Ashworth, D.C., Brown, R.J., Hansell, A.L., Fuller, G.W., 2015. Using metal ratios to detect emissions from municipal waste incinerators in ambient air pollution data. Atmos. Environ. 113, 177–186 (1994).

Galon-Negru, A.G., Olariu, R.I., Arsene, C., 2019. Size-resolved measurements of PM2. 5 water-soluble elements in Iasi, north-eastern Romania: seasonality, source apportionment and potential implications for human health. Sci. Total Environ. 695, 133839.

Gao, Y., Nelson, E.D., Field, M.P., Ding, Q., Li, H., Sherrell, R.M., Gigliotti, C.L., Van Ry, D.A., Glenn, T.R., Eisenreich, S.J., 2002. Characterization of atmospheric trace elements on PM2. 5 particulate matter over the New York–New Jersey harbor estuary. Atmos. Environ. 36, 1077–1086 (1994).

Glojek, K., Thuy, V.D.N., Weber, S., Uzu, G., Manousakas, M., Elazzouzi, R., Džepina, K., Darfeuil, S., Ginot, P., Jaffrezo, J.L., 2024. Annual variation of source contributions to PM10 and oxidative potential in a mountainous area with traffic, biomass burning, cement-plant and biogenic influences. Environ. Int., 108787

Heidari-Farsani, M., Shirmardi, M., Goudarzi, G., Alavi-Bakhtiarivand, N., Ahmadi-Ankali, K., Zallaghi, E., Naeimabadi, A., Hashemzadeh, B., 2013. The evaluation of heavy metals concentration related to PM10 in ambient air of Ahvaz city, Iran. Journal of Advances in Environmental Health Research 1, 120–128.

Hernández-Pellón, A., Fernández-Olmo, I., 2019. Airborne concentration and deposition of trace metals and metalloids in an urban area downwind of a manganese alloy plant. Atmos. Pollut. Res. 10, 712–721.

Huang, S., Tu, J., Liu, H., Hua, M., Liao, Q., Feng, J., Weng, Z., Huang, G., 2009. Multivariate analysis of trace element concentrations in atmospheric deposition in the Yangtze River Delta, East China. Atmos. Environ. 43, 5781–5790 (1994).

Hwang, S., Chi, M., Guo, S., Lin, Y., Chou, C., Lin, C., 2018. Seasonal variation and source apportionment of PM 2.5-bound trace elements at a coastal area in southwestern Taiwan. Environ. Sci. Pollut. Res. Int. 25, 9101–9113.

Idani, E., Geravandi, S., Akhzari, M., Goudarzi, G., Alavi, N., Yari, A.R., Mehrpour, M., Khavasi, M., Bahmaei, J., Bostan, H., 2020. Characteristics, sources, and health risks of atmospheric PM10-bound heavy metals in a populated middle eastern city. Toxin Rev. 39, 266–274.

In'T Veld, M., Alastuey, A., Pandolfi, M., Amato, F., Perez, N., Reche, C., Via, M., Minguillon, M.C., Escudero, M., Querol, X., 2021. Compositional changes of PM2. 5 in NE Spain during 2009–2018: a trend analysis of the chemical composition and source apportionment. Sci. Total Environ. 795, 148728.

Jena, S., Singh, G., 2017. Human health risk assessment of airborne trace elements in Dhanbad, India. Atmos. Pollut. Res. 8, 490–502.

Jiang, N., Liu, X., Wang, S., Yu, X., Yin, S., Duan, S., Wang, S., Zhang, R., Li, S., 2019. Pollution characterization, source identification, and health risks of atmospheric-particle-bound heavy metals in PM10 and PM2. 5 at multiple sites in an emerging megacity in the central region of China. Aerosol Air Qual. Res. 19, 247–271.

Koc, I., Cobanoglu, H., Canturk, U., Key, K., Kulac, S., Sevik, H., 2023. Change of Cr concentration from past to present in areas with elevated air pollution. Int. J. Environ. Sci. Technol. 1–12.

Kohonen, T., 1982. Self-organized formation of topologically correct feature maps. Biol. Cybern. 43, 59–69.

Kohonen, T., 1997. Exploration of very large databases by self-organizing maps. In: Proceedings of International Conference on Neural Networks (Icnn'97). IEEE, pp. L1–L6.

Kruskal, W.H., Wallis, W.A., 1952. Use of ranks in one-criterion variance analysis. J. Am. Stat. Assoc. 47, 583–621.

Kumar, S., Saha, N., Mohana, A.A., Hasan, M.S., Rahman, M.S., Elmes, M., MacFarlane, G.R., 2024. Atmospheric particulate matter and associated trace elements pollution in Bangladesh: a comparative study with global megacities. Water, Air, Soil Pollut. 235, 222.

Lafta, M.H., Afra, A., Patra, I., Jalil, A.T., Mohammadi, M.J., Baqir Al-Dhalimy, A.M., Ziyadullaev, S., Kiani, F., Ekrami, H.A., Asban, P., 2024. Toxic effects due to exposure heavy metals and increased health risk assessment (leukemia). Rev. Environ. Health 39, 351–362.

Li, H., Wang, J., Wang, Q., Qian, X., Qian, Y., Yang, M., Li, F., Lu, H., Wang, C., 2015. Chemical fractionation of arsenic and heavy metals in fine particle matter and its implications for risk assessment: a case study in Nanjing, China. Atmos. Environ. 103, 339–346 (1994).

Liu, X., Hadiatullah, H., Zhang, X., Trechera, P., Savadkoohi, M., Garcia-Marlès, M., Reche, C., Pérez, N., Beddows, D.C., Salma, I., 2023. Ambient air particulate total lung deposited surface area (LDSA) levels in urban Europe. Sci. Total Environ. 898, 165466.

Lucarelli, F., Calzolai, G., Chiari, M., Nava, S., Carraresi, L., 2018. Study of atmospheric aerosols by IBA techniques: the LABEC experience. Nucl. Instrum. Methods Phys. Res. Sect. B Beam Interact. Mater. Atoms 417, 121–127.

Marcazzan, G.M., Vaccaro, S., Valli, G., Vecchi, R., 2001. Characterisation of PM10 and PM2. 5 particulate matter in the ambient air of Milan (Italy). Atmos. Environ. 35, 4639–4650 (1994).

Mohammadi, M.J., Fouladi Dehaghi, B., Mansourimoghadam, S., Sharhani, A., Amini, P., Ghanbari, S., 2024. Cardiovascular disease, mortality and exposure to particulate matter (PM): a systematic review and meta-analysis. Rev. Environ. Health 39, 141–149.

Momtazan, M., Geravandi, S., Rastegarimehr, B., Valipour, A., Ranjbarzadeh, A., Yari, A. R., Dobaradaran, S., Bostan, H., Farhadi, M., Darabi, F., 2018. An investigation of particulate matter and relevant cardiovascular risks in Abadan and Khorramshahr in 2014–2016. Toxin Rev.

Mondal, S., Singh, G., 2021. PM 2.5-bound trace elements in a critically polluted industrial coal belt of India: seasonal patterns, source identification, and human health risk assessment. Environ. Sci. Pollut. Res. Int. 28, 32634–32647.

Moradi, M., Mokhtari, A., Mohammadi, M.J., Hadei, M., Vosoughi, M., 2022. Estimation of long-term and short-term health effects attributed to PM 2.5 standard pollutants in the air of Ardabil (using Air Q+ model). Environ. Sci. Pollut. Res. Int. 1–9.

Mrazovac Kurilić, S., Božilović, Z., Salem Abulsba, K., Aiad Ezarzah, A.M., 2020. Contamination and health risk assessment of heavy metals in PM10 in mining and smelting basin Bor in Serbia. Journal of Environmental Science and Health, Part A 55, 44–54.

Nakagawa, K., Yu, Z., Berndtsson, R., Hosono, T., 2020. Temporal characteristics of groundwater chemistry affected by the 2016 Kumamoto earthquake using self-organizing maps. J. Hydrol. (Amst.) 582, 124519.

Nriagu, J.O., Pacyna, J.M., 1988. Quantitative assessment of worldwide contamination of air, water and soils by trace metals. Nature 333, 134–139.

Pacyna, J.M., 1986. Atmospheric trace elements from natural and anthropogenic sources. Toxic metals in the atmosphere 33–52.

Pakbin, P., Hudda, N., Cheung, K.L., Moore, K.F., Sioutas, C., 2010. Spatial and temporal variability of coarse (PM10−2.5) particulate matter concentrations in the Los Angeles area. Aerosol. Sci. Technol. 44, 514–525.

Pant, P., Harrison, R.M., 2013. Estimation of the contribution of road traffic emissions to particulate matter concentrations from field measurements: a review. Atmos. Environ. 77, 78–97 (1994).

Park, Y., Céréghino, R., Compin, A., Lek, S., 2003. Applications of artificial neural networks for patterning and predicting aquatic insect species richness in running waters. Ecol. Model. 160, 265–280.

Parviainen, A., Casares-Porcel, M., Marchesi, C., Garrido, C.J., 2019. Lichens as a spatial record of metal air pollution in the industrialized city of Huelva (SW Spain). Environ. Pollut. 253, 918–929.

Peikertova, P., Filip, P., 2016. Influence of the automotive brake wear debris on the environment-a review of recent research. SAE Int J Mater Manuf 9, 133–146.

Pio, C., Alves, C., Nunes, T., Cerqueira, M., Lucarelli, F., Nava, S., Calzolai, G., Gianelle, V., Colombi, C., Amato, F., 2020. Source apportionment of PM2. 5 and PM10 by Ionic and Mass Balance (IMB) in a traffic-influenced urban atmosphere. Portugal. Atmos Environ 223, 117217 (1994).

Pio, C., Rienda, I.C., Nunes, T., Gonçalves, C., Tchepel, O., Pina, N.K., Rodrigues, J., Lucarelli, F., Alves, C.A., 2022. Impact of biomass burning and non-exhaust vehicle emissions on PM10 levels in a mid-size non-industrial western Iberian city. Atmos. Environ. 289, 119293 (1994).

Pokorná, P., Hovorka, J., Hopke, P.K., 2016. Elemental composition and source identification of very fine aerosol particles in a European air pollution hot-spot. Atmos. Pollut. Res. 7, 671–679.

Pyle, G.G., Swanson, S.M., Lehmkuhl, D.M., 2001. Toxicity of uranium mine-receiving waters to caged fathead minnows, Pimephales promelas. Ecotoxicol. Environ. Saf. 48, 202–214.

Querol, X., Alastuey, A., Rodriguez, S., Plana, F., Ruiz, C.R., Cots, N., Massagué, G., Puig, O., 2001. PM10 and PM2.5 source apportionment in the Barcelona Metropolitan area, Catalonia, Spain. Atmos. Environ. 35, 6407–6419 (1994).

Querol, X., Viana, M., Alastuey, A., Amato, F., Moreno, T., Castillo, S., Pey, J., De la Rosa, J., De La Campa, A.S., Artíñano, B., 2007. Source origin of trace elements in PM from regional background, urban and industrial sites of Spain. Atmos. Environ. 41, 7219–7231 (1994).

Quimbayo-Duarte, J., Chemel, C., Staquet, C., Troude, F., Arduini, G., 2021. Drivers of severe air pollution events in a deep valley during wintertime: a case study from the Arve river valley, France. Atmos. Environ. 247, 118030 (1994).

Rahman, M.S., Bhuiyan, S.S., Ahmed, Z., Saha, N., Begum, B.A., 2021. Characterization and source apportionment of elemental species in PM2. 5 with especial emphasis on seasonal variation in the capital city "Dhaka". Urban Clim 36, 100804.

Rahman, M.S., Khan, M., Jolly, Y.N., Kabir, J., Akter, S., Salam, A., 2019. Assessing risk to human health for heavy metal contamination through street dust in the Southeast Asian Megacity: dhaka, Bangladesh. Sci. Total Environ. 660, 1610–1622.

Ramos-Miras, J.J., Roca-Perez, L., Guzmán-Palomino, M., Boluda, R., Gil, C., 2011. Background levels and baseline values of available heavy metals in Mediterranean greenhouse soils (Spain). J. Geochem. Explor. 110, 186–192.

Rodriguez-Espinosa, P.F., Flores-Rangel, R.M., Mugica-Alvarez, V., Morales-Garcia, S.S., 2017. Sources of trace metals in PM 10 from a petrochemical industrial complex in Northern Mexico. Air Quality, Atmosphere & Health 10, 69–84.

Roy, D., Seo, Y., Kim, S., Oh, J., 2019. Human health risks assessment for airborne PM 10-bound metals in Seoul, Korea. Environ. Sci. Pollut. Res. Int. 26, 24247–24261.

Schauer, J.J., Lough, G.C., Shafer, M.M., Christensen, W.F., Arndt, M.F., DeMinter, J.T., Park, J., 2006. Characterization of metals emitted from motor vehicles. Res. Rep. 1–76, 77.

Seihei, N., Farhadi, M., Takdastan, A., Asban, P., Kiani, F., Mohammadi, M.J., 2024. Short-term and long-term effects of exposure to PM10. Clin Epidemiol Glob Health 27, 101611.

Sharma, K., Raju, N.J., Singh, N., Sreekesh, S., 2022. Heavy metal pollution in groundwater of urban Delhi environs: pollution indices and health risk assessment. Urban Clim. 45, 101233.

Sielski, J., Kaziród-Wolski, K., Jóźwiak, M.A., Jóźwiak, M., 2021. The influence of air pollution by PM2. 5, PM10 and associated heavy metals on the parameters of out-of-hospital cardiac arrest. Sci. Total Environ. 788, 147541.

Squizzato, S., Cazzaro, M., Innocente, E., Visin, F., Hopke, P.K., Rampazzo, G., 2017. Urban air quality in a mid-size city—PM2. 5 composition, sources and identification of impact areas: from local to long range contributions. Atmos. Res. 186, 51–62.

Sternbeck, J., Sjödin, Å., Andréasson, K., 2002. Metal emissions from road traffic and the influence of resuspension—results from two tunnel studies. Atmos. Environ. 36, 4735–4744 (1994).

Tahery, N., Geravandi, S., Goudarzi, G., Shahriyari, H.A., Jalali, S., Mohammadi, M.J., 2021. Estimation of PM10 pollutant and its effect on total mortality (TM), hospitalizations due to cardiovascular diseases (HACD), and respiratory disease (HARD) outcome. Environ. Sci. Pollut. Res. Int. 28, 22123–22130.

Tepanosyan, G., Maghakyan, N., Sahakyan, L., Saghatelyan, A., 2017. Heavy metals pollution levels and children health risk assessment of Yerevan kindergartens soils. Ecotoxicol. Environ. Saf. 142, 257–265.

Thorpe, A., Harrison, R.M., 2008. Sources and properties of non-exhaust particulate matter from road traffic: a review. Sci. Total Environ. 400, 270–282.

Vesanto, J., Alhoniemi, E., 2000. Clustering of the self-organizing map. IEEE Trans. Neural Network. 11, 586–600.

Wang, J., Hu, Z., Chen, Y., Chen, Z., Xu, S., 2013. Contamination characteristics and possible sources of PM10 and PM2. 5 in different functional areas of Shanghai, China. Atmos. Environ. 68, 221–229 (1994).

Wang, M., Lv, Y., Lv, X., Wang, Q., Li, Y., Lu, P., Yu, H., Wei, P., Cao, Z., An, T., 2023. Distribution, sources and health risks of heavy metals in indoor dust across China. Chemosphere 313, 137595.

Weber, S., Salameh, D., Albinet, A., Alleman, L.Y., Waked, A., Besombes, J., Jacob, V., Guillaud, G., Meshbah, B., Rocq, B., 2019. Comparison of PM10 sources profiles at 15 French sites using a harmonized constrained positive matrix factorization approach. Atmosphere 10, 310.

WHO, 2007. Health risks of heavy metals from long-range transboundary air pollution. https://www.who.int/publications/i/item/9789289071796.

Wilson, J.G., Kingham, S., Pearce, J., Sturman, A.P., 2005. A review of intraurban variations in particulate air pollution: implications for epidemiological research. Atmos. Environ. 39, 6444–6462 (1994).

Wu, Y., Li, G., An, T., 2022. Toxic metals in particulate matter and health risks in an E-waste Dismantling Park and its surrounding areas: analysis of three PM size groups. Int. J. Environ. Res. Publ. Health 19, 15383.

Wu, Y., Li, G., Yang, Y., An, T., 2019. Pollution evaluation and health risk assessment of airborne toxic metals in both indoors and outdoors of the Pearl River Delta, China. Environ. Res. 179, 108793.

Yang, H., Chen, J., Wen, J., Tian, H., Liu, X., 2016. Composition and sources of PM2. 5 around the heating periods of 2013 and 2014 in Beijing: Implications for efficient mitigation measures. Atmos. Environ. 124, 378–386 (1994).

Yang, W., Deng, M., Xu, F., Wang, H., 2018. Prediction of hourly PM2. 5 using a space-time support vector regression model. Atmos. Environ. 181, 12–19 (1994).

Zhong, C., Yang, Z., Jiang, W., Hu, B., Hou, Q., Yu, T., Li, J., 2016. Ecological geochemical assessment and source identification of trace elements in atmospheric deposition of an emerging industrial area: beibu Gulf economic zone. Sci. Total Environ. 573, 1519–1526.

Zhu, G., Wu, X., Ge, J., Liu, F., Zhao, W., Wu, C., 2020. Influence of mining activities on groundwater hydrochemistry and heavy metal migration using a self-organizing map (SOM). J. Clean. Prod. 257, 120664.

Ziegler, D., Malandrino, M., Barolo, C., Adami, G., Sacco, M., Pitasi, F., Abollino, O., Giacomino, A., 2021. Influence of start-up phase of an incinerator on inorganic composition and lead isotope ratios of the atmospheric PM10. Chemosphere 266, 129091.